Published in final edited form as:

Cancer Res. 2017 February 01; 77(3): 719–731. doi:10.1158/0008-5472.CAN-16-0866.

Targeting Tumor-associated Fibroblasts for Therapeutic Delivery in Desmoplastic Tumors:

——*In situ* Generation of Tumor Suppressive Fibroblasts

Lei Miao[1,*], **Qi Liu**[1,3,*], **C. Michael Lin**[1], **Cong Luo**[1], **Yuhua Wang**[1], **Lina Liu**[1], **Weiyan Yin**[3], **Shihao Hu**[4], **William Y. Kim**[2], and **Leaf Huang**[1,2,#]

[1]Division of Molecular Pharmaceutics and Center for Nanotechnology in Drug Delivery, Eshelman School of Pharmacy, University of North Carolina at Chapel Hill, Chapel Hill, NC 27599, USA

[2]Lineberger Comprehensive Cancer Center, University of North Carolina at Chapel Hill, Chapel Hill, NC 27599, USA

[3]UNC & NCSU Joint Department of Biomedical Engineering, University of North Carolina at Chapel Hill, Chapel Hill, NC 27599, USA

[4]Department of Pharmaceutics, China Pharmaceutical University, 24 Tongjiaxiang, Nanjing 210009, China

Abstract

The off-target distribution of anticancer nanoparticles (NP) to fibroblasts creates a barrier to the effective treatment of desmoplastic tumors. However, we hypothesized that this NP detriment might be exploited to target the expression of secreted cytotoxic proteins from tumor-associated fibroblasts (TAF) as an anticancer strategy. In addressing this hypothesis, plasmids encoding the secretable TNF-related factor sTRAIL were loaded into lipid-coated protamine DNA complexes (LPD) and administered by infusion in a murine xenograft model of human desmoplastic bladder carcinoma. Three doses were sufficient to generate ~70% of TAFs as sTRAIL-producing cells. sTRAIL triggered apoptosis in tumor cell nests adjacent to TAFs. Further, it reverted residual fibroblasts to a quiescent state due to insufficient activation, further compromising tumor growth and remodeling the microenvironment to favor second-wave nanotherapy. We confirmed the efficacy of this strategy in an orthotopic xenograft model of human pancreatic cancer, where the desmoplastic stroma is well-known to be a major barrier to the delivery of therapeutic NP. Collectively, our results offer a proof of concept for the use of NP to modify TAFs as an effective strategy to treat desmoplastic cancers.

Edited Precis

Results offer a preclinical proof of concept for the use of nanoparticles to modify tumor-associated fibroblasts as a strategy to treat desmoplastic cancers.

[#]To whom correspondence should be addressed. Leafh@email.unc.edu.
[*]Contributed equally.

There's no conflict of interest to disclose

Keywords

tumor-associated fibroblast; TRAIL; nanoparticle; desmoplastic tumor

Introduction

The enhanced permeation and retention (EPR) effect describes the increased intra-tumoral accumulation and cellular uptake of therapeutic nanoparticles (NPs) in oncology, demonstrating promising preclinical responses (1). Unfortunately, the early promise of several therapeutic NPs has failed to translate clinically (2). One of the major mechanisms is the heterogeneous uptake of drugs or NPs in neighboring stromal cells (3). Tumor-associated macrophages (TAMs) are a major off-target depletion site for NPs (2,4). Additionally, in tumors with desmoplastic stroma, tumor-associated fibroblasts (TAFs) that wrap around blood vessels, constitute another barrier for tumor-specific NP delivery (1,5).

Off-target distribution of therapeutic NPs can result in adverse effects (6). Depletion of stromal cells has been proposed to circumvent stroma-induced adverse effects and improve tumor cells' capture of therapeutic agents (7,8). However, this strategy has many limitations. Firstly, it runs the risk of eliminating stromal components needed for tissue homeostasis, paradoxically facilitating metastasis (9). We also found that TAFs damaged by a nano-formulation of cisplatin could produce survival factors, such as Wnt16 to support the proliferation of tumor cells (5). In addition, significant heterogeneity appears to be in the type of stroma within tumors, with some stroma being tumor-suppressive and some pro-tumorigenic (10). Stromal components can produce small proteins (e.g. cytokines) secreted *in situ*, which can bypass stromal cells barriers and bind avidly to targeted cells causing overexpression of their receptors (11). Since cytokines can modulate tumor growth, we sought to engineer an *in situ* stromal depot capable of secreting cytotoxic cytokine-like proteins, as an alternative stroma modulating strategy to constrain the growth of desmoplastic tumors.

The best way to generate this theoretical stromal depot is gene therapy, as it allows proteins to be produced locally at higher rates and more quantities than through systemic delivery of recombinant proteins (12). While the off-target delivery of therapeutic NPs traditionally compromises the efficacy of tumor-specific treatments, this phenomenon can be exploited to specifically deliver genes to stroma cells, thus providing the basis for *in situ* synthesis and secretion. Since macrophages and fibroblasts are the major off-target sites in desmoplastic tumors, they are excellent candidates for *in situ* reprogramming. However, expression of plasmids in macrophages is limited by the macrophages' natural enzymes for plasmid degradation (13). In addition, the regeneration of macrophage or other circulating monocytes limits the persistency of gene expression (1). Therefore, TAFs, as a locally recruited cell population, may serve as a more suitable protein-producing reservoir.

TNF-related apoptosis-inducing ligand (TRAIL) efficiently induces apoptosis in a wide range of tumor cells while sparing normal cells, making it an ideal candidate for cancer therapy (14). Full-length TRAIL is a transmembrane protein lacking a leader sequence for extracellular secretion (12). Its apoptotic effects are limited to cells near the plasmid

transfected cells, compromising the therapeutic efficacy (15). Thereby, a secretable form of TRAIL (sTRAIL) was engineered. sTRAIL consists of an extracellular domain of TRAIL fused with an NH_2-terminal extracellular domain of Flt3L, a ligand for flt3 tyrosine kinase receptor that aids in secretion (16). It was then necessary to utilize the off-target distribution of NPs to target sTRAIL-containing NPs toward fibroblasts, seeking to make them tumor-inhibitive in desmoplastic tumors. The utilization of TRAIL-resistant low proliferating fibroblasts as a gene-producing reservoir has two important advantages: (a) allowing a comparatively long gene expression compared to sensitive tumor cells and (b) maintaining the stroma cell components for tissue homeostasis.

To confirm this proof of concept, a *stroma-vessel* desmoplasia model was established by co-inoculating UMUC3 bladder cancer cells with NIH3T3 fibroblasts. Lipid-coated protamine DNA complexes (LPD) were developed and utilized for encapsulating sTRAIL plasmids. The fibroblasts' expression of sTRAIL and the apoptosis of neighboring tumor cells were assessed. The concept was further evaluated with a clinically relevant, TRAIL sensitive, orthotopic desmoplastic PDAC model of BXPC3. As expected, the *in situ* expression of sTRAIL by fibroblasts induced potent tumor inhibition. However, residual TAFs unexpectedly reverted to quiescence, presumably due to death of neighboring tumor cells. This led to the remodeling of tumor microenvironment (TME) and provides a new paradigm for a second-wave nanoparticle therapy.

Materials and Methods

Cell lines, animals, and antibodies

The mouse embryonic fibroblast cell lines NIH3T3 and the human lung fibroblasts MRC-5 were purchased from UNC Tissue Culture Facility. The human bladder transitional cell line UMUC3 was provided by Dr. William Kim. The human pancreatic cancer BXPC3-Luc2 was purchased from PerkinElmer (Waltham, MA). UMUC3 and NIH3T3 were maintained in Dulbecco's Modified Eagle's Media (Invitrogen, CA), supplemented with 10% fetal bovine serum (FBS) (Sigma, MO) or 10% bovine calf serum (Sigma, MO). BXPC3-Luc2 cells were cultured in full RPMI-1640 medium (Invitrogen, CA), while MRC-5 were cultured in full αMEM (Invitrogen, CA). Cell lines were authenticated by Dr. William Kim's group and UNC Tissue Culture Facility using the Short Tandem Repeat (STR) profiling method. Female nude mice 6–8 weeks-old were obtained from and raised by the University of North Carolina animal facility. All animal handling procedures were approved by the University of North Carolina at Chapel Hill's Institutional Animal Care and Use Committee. Primary and secondary antibodies used for Western blot (WB), flow cytometry (flow cyt), immunofluorescence staining (IF), and immunohistochemistry (IHC) staining are listed in Table S1.

Preparation and characterization of LPD

LPD were prepared through a stepwise self-assembly process based on previous protocols (17). Briefly, DOTAP and cholesterol (1:1, mol/mol) were dissolved in chloroform, and the solvent was removed. The lipid film was then hydrated with distilled water to make the final concentration of 10 mmol/L cholesterol and DOTAP. Then, the liposome was extruded

through 200 nm and 100 nm polycarbonate membranes (Millipore, MA) to form 70–100 nm unilamellar liposomes. The LPD polyplex cores were formulated by mixing 140 μL of 36 μg protamine in 5% glucose with equal volume of 50 μg plasmid in 5% glucose. The mixture was incubated at room temperature for 10 min and then 60 μL cholesterol/DOTAP liposomes (10 mmol/L each) were added. Post insertion of 15% DSPE-PEG and DSPE-PEG-AA was performed at 60 °C for 15 minutes. The size and surface charge of the NPs were determined by a Malvern ZetaSizer Nano series (Westborough, MA). TEM images were acquired using a JEOL 100 CX II TEM (JEOL, Japan).

sTRAIL and TRAIL construction

The p-sTRAIL containing genes encoding a Flt3L leader sequence, isoleucine zipper, the extracellular domain of TRAIL, followed by an internal ribosome entry site (IRES) and GFP under a CMV promoter were previously constructed and provided by Dr. Shawn Hingtgen (University of North Carolina at Chapel Hill, NC). To establish the p-TRAIL construct, the sTRAIL sequence was cleaved from the p-sTRAIL vector via digesting with XhoI/BamHI (New England Biolabs, CA). The full length TRAIL cDNA was amplified by PCR using a sense primer containing the XhoI site (5'-CAGCCTCGAGCGACCATGGCTATGATGGAGGTC-3') and an antisense primer containing the BamHI site (5'-CAGCGGATCCTTAGCCAACTAAAAAGGCCCCG-3'). The amplified DNA was digested with XhoI/BamHI, and inserted into the XhoI/BamHI site of the pre-removed p-sTRAIL construct. The insertion was confirmed by double digestion and PCR. The sequence was verified using Applied Biosystems 3730×l Genetic Analyzers.

Tumor growth inhibition

The UMUC3/NIH3T3 model was established as previously reported with little modification (18,19). In brief, UMUC3 cells (5×10^6) and NIH 3T3 cells (2.5×10^6) were subcutaneously co-inoculated into the right flank of mice with Matrigel (BD Biosciences, CA). Treatments were initiated on the 11th day when tumor sizes reached ~500 mm^3. Mice were then randomized into 4 groups (n~7 per group) as follows: Untreated group (PBS), GFP LPD, TRAIL LPD, and sTRAIL LPD. IV injections were performed every other day for a total of 4 doses of 50 μg plasmid/mouse. Tumor volume (1/2*length*length*width) was measured every day with a digital caliper (Thermo Fisher Scientific, PA) and body weight was also recorded. The desmoplastic BXPC3-Luc2 model was established by orthotopic injection of 1×10^6 cells into the tail of the pancreas. Injections of LPDs were started 15 days after inoculation and dosed every 2 days, for a total of 4 times. Tumor growth was monitored using IVIS® Kinetics Optical System (Perkin Elmer, CA) twice a week. The increases of tumor volumes were calculated as the radiance of the intensities.

Flow cytometry analysis

To study the cell population that took up NPs within tumors, mice were injected with DiI-labeled LPD (0.1 mg/kg DiI) and were sacrificed at determined time post-intravenous injection. Fresh tumor tissues were dissociated with 1 mg/mL collagenase (Invitrogen), 1 mg/mL hyaluronidase (Sigma, MO) and 200 μg/mL DNAase (Invitrogen, CA) in DMEM/2% FBS, 40 min to generate a single cell suspension. The fibroblasts were pre-transfected with green fluorescence protein (GFP). Leukocytes were stained with APC-

conjugated CD45 antibody. The cells were then subjected to flow cytometry analysis after washing. The ratios of DiI-labeled NPs distributed in different cell populations were then calculated.

To analyze the expression of IRES GFP in fibroblasts and other cells within the bulk tumor, tumor tissues were collected after single-dose or multiple-dose treatments. Tumor tissues were dissociated, and the ratio of GFP-expressed fibroblasts (RFP-fibroblasts in UMUC3/3T3 model or αSMA positive fibroblasts in BXPC3 model) in the dissociated cells was analyzed by flow cytometry on a BD FACS Aria instrument (Beckon Dickinson, CA).

To quantify the expression of TRAIL and TAF markers in RFP-fibroblasts of the UMUC3/3T3 model, the dissociated cells were sorted using MoFlo XDP (Beckman Coulter, CA), and the collected fibroblasts and other cells were processed through RNA extract, DNA reversion, and qPCR analysis.

Statistical analysis

Statistical analysis was undertaken using Prism 5.0c Software. A two-tailed t-test or a one-way analysis of variance (ANOVA) was performed when comparing two groups or more than two groups, respectively. Statistical significance was defined by a value of $P < 0.05$. Data were shown as mean ± SD.

Additional methods

Detailed methodology including materials, gene transfection, cell viability assay, Quantitative Real-time PCR (qPCR) Assay, ELISA, western blot, IF and IHC, etc. are described in the Supplementary Methods.

Results

Identification of fibroblasts as the major off-target cells for LPD uptake within a *stroma-vessel* desmoplastic tumor model

LPD NPs were prepared according established protocols with few adjustments (5). Anisamide was conjugated onto the surface of NPs as a ligand for cells overexpressing the sigma receptor (including tumor cells and TAFs). A secondary amine 2 carbons away from the amide carbon was added to the anisamide structure (DSPE-PEG-SP2-AA) to ensure enhanced binding affinity and specificity according to the previous report (20,21). The final NPs were ~70 nm in diameter, with a surface charge of ~25 mV (Table S2). TEM images confirm the size of LPD and indicate its spherical shape and homogenous distribution (Fig. S1). 0.5% DiI was incorporated into the lipid membrane as an *in vivo* tracker of LPD.

A *stroma-vessel* type (a common stroma architecture in desmoplasia) desmoplastic tumor model was generated from simultaneous subcutaneous inoculation of UMUC3 bladder cancer cells along with NIH3T3 fibroblasts (UMUC3/3T3) (Fig. 1A). Histopathology demonstrates an anatomical vicinity between blood vessels and tumor-associated fibroblasts within the UMUC3/3T3 xenografts (Fig. 1A and Fig. S2). DiI-labeled LPD reached UMUC3/3T3 tumors within 10 h of intravenous injection, and plateaued over 48 h (Fig. S1C). Consistent with other NPs of similar size, liver and spleen were the major LPD

accumulating organs. Flow cytometry was performed to determine LPD accumulation in various cell populations within the tumor. Stable expression of GFP and fluorophore conjugated antibody against mouse CD45 defined fibroblasts and leukocytes populations, respectively. Results showed that ~27% of the cells within the bulk tumor were fibroblasts (GFP positive) while ~16% were $CD45^+$ leukocytes. The majority of remaining cells, as shown in a previous study, were tumor cells (Fig. 1B) (5). More than ~60% of fibroblasts (GFP positive) took up LPD at 10 h post intravenous injection, accounting for ~65% of the total NP-associated cells (Fig. 1C and D, Fig. S3). Despite gradual clearance or degradation of the fluorescent NPs, ~20% of fibroblasts still remained DiI positive 72 h after injection. In contrast, only ~20% of the $CD45^+$ leucocytes initially took up DiI LPD. Furthermore, less than 10% of tumor cells took up NPs during any of the time points assayed. These analyses ultimately indicate that fibroblasts are the major off-target cells responsible for LPD uptake in the *stroma-vessel* desmoplastic tumors.

In vitro transfection of fibroblasts with sTRAIL in LPD induces apoptosis of neighboring tumor cells

A bioactive, secretable form of trail was constructed by Hingtgen et al., through fusing coding sequences for the extracellular domain Flt3L (a.a1–81) and an isoleucine zipper to promote trimerization, with the a.a114–281 of trail (22,23). p-TRAIL encoding the human full-length trail and p-GFP were constructed as controls (Fig. 2A). To monitor the cellular origin of the gene expression, intracellular protein GFP was co-expressed with sTRAIL or TRAIL through the internal ribosomal entry site (IRES) sequence (Fig. 2A). The plasmid constructs were encapsulated into LPD. Particle size and zeta potential remained constant regardless of the type of plasmid encapsulated (Table S1). qPCR analysis suggested that the expression efficiency of sTRAIL LPD and TRAIL LPD, as indicated by the relative mRNA levels of the extracellular domain of TRAIL (TRAIL(ex)), were similar in the activated NIH3T3 (pre-conditioned with TGF-β to obtain TAF-like phenotypes), and comparable with those delivered via Lipofectamine®-2000 (Fig. S4).

TRAIL activates the Caspase 3/8 dependent apoptosis response in epithelial-derived cells [35]. Indeed, we found that the viability of UMUC3 transfected with TRAIL or sTRAIL, but not GFP, was drastically decreased (Fig. 2B). No significant difference was observed between cells treated with TRAIL or sTRAIL, most likely due to the sufficient transfection of cells. Therefore, secretion was not a limiting step *in vitro* for cytotoxicity [36]. Normal fibroblasts (e.g., murine NIH3T3, or human MRC-5) were resistant to the TRAIL, likely from the overexpression of decoy receptors or an alternate downstream pathway (15). The secretion of TRAIL was then evaluated in the supernatant of activated NIH3T3 pre-transfected with different plasmids. Consistent with previous studies, abundant sTRAIL was detected in media by ELISA Assay, while the concentration of full-length TRAIL was ~50 times lower in media, suggesting that the leader sequence is essential for sTRAIL release (Fig. 2C) [28]. Next, sTRAIL released into the culture media was assayed for biological activity (Fig. S5). The growth media for UMUC3 were replaced with culture supernatants from NIH3T3 cells transfected with sTRAIL, TRAIL, or GFP. The culture supernatant containing sTRAIL, but not TRAIL, exerted a significant cytotoxic effect on UMUC3. The neighboring effect was further confirmed by non-direct contact co-culture (Fig. 2D).

UMUC3 (bottom layer) was co-cultured with activated fibroblasts (upper chamber) preloaded with different plasmids. The total cell number was significantly lower in the sTRAIL co-culture group. Further, ~13.2% early apoptosis and ~6.7% late apoptosis were observed in the sTRAIL co-culture group as compared to other treatment groups (Fig. 2D). All together, these data verify the prerequisites for *in situ* gene modification of fibroblasts: (a) fibroblasts are resistant to both sTRAIL and TRAIL, while tumor cells are sensitive to them; (b) sTRAIL can be efficiently released within the supernatant; and (c) the neighboring effect thereby occurs instantly.

Secreted TRAIL induces superior antitumor efficacy in the *stroma-vessel* desmoplastic bladder cancer model

The efficacy of systemically delivered sTRAIL was evaluated using the UMUC3/3T3 model. Treatment began when tumor sizes reached 500 mm^3, allowing the *stroma-vessel* structure to form. Equal amounts of plasmids in LPDs were intravenously injected into mice. As shown in Fig. 3A, the tumor growth in mice treated with sTRAIL LPD was significantly inhibited compared to other groups. GFP-LPD exhibited a slight antitumor effect, likely from the non-specific induction of inflammatory cytokines from the cargos and DNA backbones (24). To demonstrate the neighboring effect induced from sTRAIL, the full-length TRAIL LPD was administered as a less secretable control. As expected, full-length TRAIL showed minimal antitumor efficacy compared to sTRAIL. qPCR analysis of the mRNA expression using primers (Fig. S4, Table S3) for TRAIL(ex) suggested comparable expression of sTRAIL and TRAIL in tumors treated with 4 doses of LPDs (Fig. 3B). This, in conjunction with the *in vitro* transfection data (Fig. S4), which indicated a similar transfection efficiency between these 2 plasmids, and thus dismissed the possibility that a difference in expression levels between sTRAIL and TRAIL affect the antitumor effect. Notably, both TRAIL and sTRAIL LPD induced >7 times greater expression of TRAIL(ex) compared to the PBS-treated group with a baseline level of endogenous TRAIL. Additionally, the expression of mRNA persisted at least 4 days after the endpoint dose, suggesting relatively long gene expression profiles. qPCR assay using primers specific for sTRAIL confirms the expression of sTRAIL plasmid (Fig. S6). With a lower baseline level compared to TRAIL(ex) mRNA, the relative sTRAIL production was ~200 times higher relative to the control. The expression and secretion of TRAIL protein were further examined in the UMUC3/3T3 xenografts. Dissociated cells from the treated tumors were cultured and the conditioned media (secretomes) were measured by ELISA for TRAIL protein (both normal TRAIL and sTRAIL). Indeed, tumors from sTRAIL LPD treated animals secreted more TRAIL protein than any other groups including the ones treated with TRAIL LPD (Fig. S7). Results indicate the strong potency of gene transfection and protein secretion by using LPD, and suggest a promising therapeutic outcome of sTRAIL LPD in treating the desmoplastic UMUC3/3T3 tumors (Fig. 3A).

The sTRAIL LPD were delivered to and expressed in fibroblasts *in situ*

Next, we assessed the loco-regional expression of sTRAIL in different cell populations within the tumors. Since the intracellular protein GFP was fused with sTRAIL through an IRES sequence, the cells that expressed GFP represented cells that secrete sTRAIL. Moreover, to visualize the fibroblasts, RFP expressing NIH3T3 cells were co-inoculated

with UMUC3 cells. Notably, the xenograft developed from UMUC3 cell lines alone had minimal to no endogenous fibroblasts (19). Therefore, the RFP-fibroblasts constituted the majority of fibroblast populations in the UMUC3/3T3-RFP model. As shown in Fig. 3C–F, mice treated with a single dose of sTRAIL LPD exhibited moderate GFP expression, exclusively localized within the RFP-fibroblasts. The strongest GFP expression was elicited after 4 doses of NPs. The expression of GFP was quantitatively confirmed using flow cytometry (Fig. 3G). Consistently, overall expression of GFP increased dose dependently, but the majority of expression was limited to RFP-fibroblasts.

This data confirmed that fibroblasts were the major reservoir for *in situ* generation of LPD-delivered proteins. This was most likely due to off-target distribution of NPs and relatively high and stable expression of genes in fibroblasts compared to other off-target cell populations (e.g., macrophages). Notably, the expression of GFP in other cells were observed two days after the endpoint dose (Fig. 3F and G), suggesting that a portion of NPs had overcome the fibroblast-elicited barriers and entered into the tumor nest. However, the expression of GFP in this group of cells decreased dramatically 4 days after the endpoint injection while the expression in fibroblasts remained constant (Fig. 3G). There are two hypothesized mechanisms related to these observations: (a) the tumor cells may internalize the NPs but undergo apoptosis immediately, or (b) the infiltrating leukocytes take up the NPs, but cells escaped into the circulate afterwards. Either cell population demonstrated transient expression of the genes compared with local TRAIL-resistant fibroblasts, confirming fibroblasts as the most suitable engineered reservoir. The expression levels of sTRAIL mRNA were further assayed in the RFP-fibroblasts sorted from tumors with three doses of sTRAIL or GFP LPD (Fig. 3H). As expected, only the fibroblasts treated with sTRAIL LPD elicited the synthesis of sTRAIL mRNA.

Neighboring effect unveiled the apoptotic effect of TRAIL in the *stroma-vessel* desmoplastic bladder cancers

The distribution of apoptotic cells was then examined using a terminal deoxynucleotidyl transferase dUTP nick end labeling (TUNEL) assay on the UMUC3/3T3 model (using wild type unlabeled fibroblasts). TAFs were simultaneously visualized by staining with αSMA. Only a trace amount of TUNEL-positive cells was observed after single dose of sTRAIL LPD, the majority of which was localized near αSMA-positive TAFs (Fig. 4A). The apoptotic area grows around αSMA positive TAFs as the doses increase. Sections from different tumors after each dose were then analyzed to quantify the average distances between apoptotic cells and the nearest αSMA-positive TAFs. Consistent with the fluorescence images, the distribution radius of apoptotic cells increases with dose and over time (Fig. 4B). The data substantiate the claim that a neighboring effect of fibroblasts is indeed present in fibroblasts *in situ*, facilitated by diffusion, and amplified with escalated dosing schedules. The apoptotic assay was also performed in other treatment groups after the endpoints (Fig. 4C). As expected, minimal apoptosis was observed in the PBS and GFP-LPD group, whereas a small amount of TUNEL-positive nuclei were observed in groups treated with TRAIL LPD. We hypothesized that the proteolytically cleaved extracellular domain of the full-length TRAIL induced apoptosis of neighboring tumor cells, or a paucity of NPs diffused through the TAF-layer, inducing the synthesis of TRAIL and apoptosis in

neighboring tumor cells, thus explaining the limited apoptotic cells observed in the TRAIL LPD near TAFs. In comparison, an extensive amount of apoptotic cells was observed in the sTRAIL LPD group. In addition, the residual fibroblasts (especially TAFs) were clustered, sparing any tumor nest structure. Potent, well-dispersed apoptosis along with this disordered and clustered fibroblast structure suggested a tumor microenvironment less structurally and functionally capable of growth and progression, thus verifying the superior antitumor activity of sTRAIL LPD compared to other treatments.

Apoptosis of neighboring tumor cells induced by sTRAIL LPD causes reprogramming of residual fibroblasts, facilitating the delivery of second-wave therapeutic NPs

We next examined the function of residual fibroblasts. The levels of collagen, a major extracellular matrix (ECM) protein, were assessed after multiple sTRAIL treatments in mice bearing UMUC3/NIH3T3 (25). Unexpectedly, the collagen content decreased ~3-fold compared to other treatment groups (Fig. 5A and B). Collagen level within TME under sTRAIL LPD treatment was also monitored (Fig. S8). Results indicated a gradual reduction of collagen level in response to sTRAIL treatment. Reductions were also observed on other proteins unique to fibroblast activation of functional significance in the TME, including fibronectin and hepatocyte growth factor (HGF) (Fig. 5C) (5,9,26). In addition, fibroblast activation markers, αSMA and fibroblast activation protein alpha (FAPα) decreased by ~90% and ~84% (compared to total RFP-fibroblasts), respectively (Fig. 5C) (5,9,27). These data suggested that residual TAFs were shifted from an activated to a quiescent state. However, the proteins (i.e., FAPα and fibronectin) described above are not exclusively secreted by fibroblasts (28,29). To further confirm the state shift of fibroblasts, we sorted the RFP-fibroblasts from the dissociated cells collected from tumors after 3 doses of sTRAIL LPD. Indeed, we found the mRNA level of COL1A1 (collagen) and ACTA2 (αSMA) in sTRAIL treated fibroblasts decreased ~2 to 5-fold compared to untreated fibroblasts (Fig. 5D). Meanwhile tumors treated with full-length TRAIL or GFP-LPD failed to affect desmoplasia, eliminating any possibility of TRAIL directly inducing fibroblast reprogramming (Fig. 5A–D). Since it is commonly accepted that the majority of TAFs are transdifferentiated from resident fibroblasts in response to TGF-β (30), the downstream portions of TGF-β signaling, including pSMAD2 and plasminogen activator inhibitor type 1 (PAI-1) were examined (27,30,31). Indeed, data revealed a decreased level of pSmad2 nuclei staining and an inhibition of the transcriptional activation of PAI-1 in fibroblasts of sTRAIL treated tumors (Fig. 5D and E). Again, the data support the reprogramming of TAFs (9).

We next assessed the response of intratumoral blood vessels to the normal stroma restoration and the neoplastic cell loss. Both the vascular density and vessel diameter were observed and quantified in mice bearing UMUC3/3T3 xenografts (Fig. 5F and Fig. S9 A and B). There was no significant increase in vessel density associated with any of the treatments, suggesting no obvious angiogenesis effects. In fact, the vessel density decreased in some sTRAIL or TRAIL treated mice, likely due to the inhibition of the proangiogenic factor, VEGF, through reduced mRNA expression. Yet this effect was not statistically significant (32). Whereas, sTRAIL, not TRAIL LPD profoundly increased the blood vessel diameter and vessel lumen size (Fig. 5F and Fig. S9). This finding indicates that sTRAIL LPD could effectively decompress the intratumoral vasculatures (33), leading to the normalization of

blood vessels. Normalized vasculatures are often characterized by uncompressed vessels with greater pericytes coverage (34,35). Indeed, the loosely attached or absent pericytes in tumor vessels were replaced with compact, normalized pericytes after sTRAIL LPD treatment (Fig. S9G). Further, these morphological changes were accompanied by functional changes, *i.e.* the increased tumor oxygenation, as indicated by the rapid downregulation of the hypoxia-inducible factor 1 alpha (HIF 1α) (36) after sTRAIL LPD treatment (Fig. S9D) (34,37). The normalization of blood vessels and restoration of normal stroma would ultimately lead to reduction of the interstitial fluidic pressure as indicated by studies reported elsewhere (34,35).

Since normalized blood vessels with reduced IFP and hypoxia were characterized and reported, it was then questioned whether the remodeled TME would ultimately increase the accumulation, penetration and efficacy of second-wave nanocarriers: which describes an additional course of chemotherapy following TME modulation (38). Lipid-coated cisplatin nanoparticles (LPC NPs, ~30 nm) were previously developed in our lab and used for the tumor accumulation study herein. Detailed characterizations of the NPs have been described by Guo et al (39). Indeed, pre-treatment of the tumors with sTRAIL LPD led to a ~2-fold increase of cisplatin retention 24-h-post a single-dose intravenous injection of cisplatin NPs (Fig. 5G and H). The intratumoral distribution of cisplatin NPs were visualized using DiI-labeled cisplatin NPs. As it shown in Fig. 5J, normalization of blood vessels after sTRAIL treatment efficiently improved the extravasation and penetration of small NPs. To demonstrate the possible therapeutic benefits of the two-wave therapy, mice were first pretreated with 3 doses of sTRAIL LPD, as shown in Fig. 5G. Results herein suggest that the two-wave therapy significantly inhibited and delayed the tumor growth more than single modality therapy (Fig. 5I). In conclusion, the data suggest residual fibroblasts and TME after sTRAIL treatment are remodeled, benefiting not only the sTRAIL-mediated antitumor efficacy, but also the delivery of a second-wave chemotherapy.

In situ engineering of pancreatic stellate cells with sTRAIL LPD NPs shows promising antitumor efficacy in an orthotopic desmoplastic pancreatic cancer BXPC3

To evaluate if the above-mentioned findings could be recapitulated in tumors that are clinically known to have extremely high desmoplastic fibrosis, the anti-tumor efficacy of sTRAIL LPD was assessed on mice bearing the human pancreatic adenocarcinoma BXPC3. BXPC3 are *stroma-vessel* type desmoplastic tumors characterized with nests of tumor cells surrounded by vessel-embedded fibrotic tissues (Fig. S10) (40–42). The cultured BXPC3 had greater sensitivity to TRAIL compared to other pancreatic cancer cell lines (43). To visualize tumor growth *in vivo*, BXPC-3 cells were stably transfected with luciferase vector (BXPC3-Luc2). BXPC3-Luc2 was orthotopically injected into the tail of the pancreas. The dosing schedule of sTRAIL LPD is presented in Fig. 6A. Tumor volume correlated from the number of photons emitted from the tumor were assessed (Fig. 6B) and quantified (Fig. 6C). Results demonstrated that sTRAIL LPD, but not other treatment groups effectively inhibited tumor growth. Further, of all mice treated with different regimens, only sTRAIL treatment significantly improved the overall survival. Mean survival time (MST) was increased to 65 days as compared to other treatment groups (43, 50, and 53 days for PBS, GFP LPD and TRAIL LPD groups, respectively, Fig. 6D), conveying a potent therapeutic effect and a

prolonged survival effect. Major organs were imaged for metastasis and results were presented in Fig. S11. Results demonstrated that, sTRAIL LPD treatment also efficiently ameliorated tumor metastasis (primarily to liver and lung). To verify that the hypothesis regarding *in situ* engineering of fibroblasts occurred in the BXPC3 model, the expression of GFP (the IRES-GFP from sTRAIL and TRAIL LPD or GFP from GFP LPD) in fibroblasts and other cells was examined. Indeed, more than ~25% of fibroblasts expressed GFP, accounting for ~40% of the total GFP expressing cells (Fig. 6D). In addition, only ~8% of the $CD45^+$ leucocytes expressed GFP (Fig. S12). This, again, supports the claim that fibroblasts are the primary engineered population for sTRAIL secretion. To verify that fibroblasts induced neighboring effect and the remodeling of TME, the post-treatment apoptosis and collagen level are shown in Fig. 6E–G. Consistently, an increased amount of TUNEL-positive cells was localized near fibroblasts. The overall level of collagen in the non-scar tissue area decreased. Heterogeneities, particularly the extensive extracellular matrix with few viable cells (the scar tissue) (44) was primarily observed in the sTRAIL LPD tumors (Fig. S13) due to the efficient elimination of tumor cells by sTRAIL. Normalization of blood vasculatures and reduction of tumor hypoxia were also found in the sTRAIL LPD tumors (Fig. S14). Once again, the results clearly demonstrate that *in situ* engineering of fibroblasts benefits anti-cancer therapy in *stroma-vessel* desmoplastic tumors.

Toxicity evaluation for the different treatments and blood chemistry analysis

Toxicological evaluation demonstrated little to no noticeable morphological changes in organs where LPD NPs are distributed (e.g., liver and spleen) (Fig. S14A and B). The serum biochemical value analysis demonstrated that the sTRAIL treatment group had no liver (aspartate aminotransferase and alanine aminotransferase) or kidney (creatinine and blood urea nitrogen) toxicity caused by tumor progression (Table S4). One possible mechanism is that, though liver is the major site for NP accumulation, ~65% of the NPs were actually trapped in CD68 positive Kupffer cells with low plasmid expression (Fig. S14 D–F) (45). Tumors were the mainly plasmid transfection and protein synthesis reservoir (Fig. S14 D–E). In addition, hematology study showed no significant bone marrow suppression in sTRAIL treated mice compared to the control groups, suggesting the treatment did not cause anemia (Fig. S14B).

Discussions

Despite recent advances in nano-therapeutics, efficacy against desmoplastic tumors, including pancreatic cancer and advanced urothelial carcinoma, has not changed in decades (9). In part, the dense stromal barrier captures NPs, preventing them from reaching the tumor (1,19). Given the large amount of NPs delivered to fibroblasts, we hypothesized that we could take advantage of this natural property of bladder and pancreatic cancers and target cancer treatment through fibroblasts. Inspired by fibroblast's ability to secrete tumor supportive cytokines to neighboring tumor cells (46,47), modification of fibroblasts to secrete tumor suppressive cytokines through gene delivery with NPs was proposed in the current manuscript. The *in situ* engineering of fibroblasts harnesses the location of fibroblasts between blood vessels and tumor cells, bypassing major cellular barriers for NP

delivery; subsequently converting fibroblasts from a tumor supporting role to a tumor depletion center.

The choice of the secretable tumor suppressive factor should not be understated. TRAIL is a highly selective, tumor apoptosis-inducing cytokine. The resistance of mesenchymal stroma cells, especially fibroblasts to TRAIL was a conceivable mechanism for the clinical failure of TRAIL (15). However, this feature demonstrates fibroblasts as a durable synthesis reservoir for TRAIL, with prolonged expression compared to other TRAIL-sensitive cells. In reality, TRAIL-secreting human mesenchymal stem cells have been used for prolonged delivery of TRAIL in glioma (48). In order to achieve the original hypothesis, TRAIL was fused with a leader sequence into a bioactive secretable form (sTRAIL). Despite the comparable cytotoxicity observed *in vitro* with both sTRAIL and TRAIL plasmid, only sTRAIL encapsulated in LPD induced superior antitumor efficacy in desmoplastic tumors. Consistent with *the in situ fibroblast engineering* hypothesis, we found the majority of sTRAIL was expressed within fibroblasts within 3 doses of sTRAIL LPD. The penetration of sTRAIL protein is another concern for the *in situ* engineering. Compared to most monoclonal antibodies, the trimerized sTRAIL with a smaller molecular weight offered rapid diffusion. The current work illustrated that apoptotic tumor cells induced by sTRAIL LPD can be observed 500 μm away from the nearest fibroblast (Fig. 4). Compared to the average diameter (400 μm) of tumor nests in the UMUC3/3T3 model, the depth of penetration was undoubtedly sufficient to induce potent efficacy.

The apoptosis of tumor cells destroyed the nest structure, keeping fibroblasts as the major population of remaining cells. A quiescent characteristic marked by a reduction in ECM protein synthesis and decreased TAFs marker expression in the residual fibroblasts was found only after sTRAIL treatment. Down regulation of pSMAD2 in fibroblasts suggested this process may be mediated by TGF-β (30,49). Though further mechanistic studies should be conducted, the original hypothesis stated the apoptosis of neighboring tumor cells reciprocally reprograms TAFs due to insufficient TGF-β signaling activation. To verify this hypothesis, an experiment was conducted *in vitro* consisting of a non-contact co-culture of 3T3 cells secreting sTRAIL with UMUC3 tumor cells. Indeed, we found significant correlation between decreased fibroblast αSMA markers and increased tumor cell apoptosis (Fig. S15). Support for this hypothesis can also be found in that pSMAD was also downregulated in apoptotic tumor cells *in vivo*, which was mediated through autocrine signaling of TGF-β. In addition to the apoptotic tumor cells, the apoptosis-induced recruitment of pro-inflammatory cells responsible for TAF reprogramming would be an additional source of the stroma remodeling. This particular mechanism will be evaluated in the future studies. Additionally, the phenotype of fibroblasts in TRAIL treatment group remained constant, demonstrating TRAIL had minimal direct effect on fibroblasts.

Reverting of TAFs has a dual benefit. Firstly, the cellular and structural changes of the stroma resulted from “normalized” fibroblasts are reported to exert tumor-suppressive forces and signals, potentially inhibiting tumor growth (9,50). Secondly, the reduction of the fibrotic content, which decompresses the intratumoral vasculature, creates a window for the second-wave nanotherapy (9,34). Such expectations were presented both in theory and in the

current study. Treatment with sTRAIL LPD significantly enhanced the delivery, retention, penetration and efficacy of additional cisplatin NPs.

Moreover, the potency of sTRAIL LPD monotherapy, observed on a hypovascular orthotopic pancreatic carcinoma (BXPC3) further verified the feasibility of this *in situ* engineering approach. The result is promising, as only a small population of therapeutic NPs have shown efficacy against PDACs.

Collectively, a novel regimen for the treatment of desmoplastic tumors was developed by utilizing their off-target uptake of NPs to our benefit (Fig. 7). Three advantages highlight the sophistication of this approach: (1) the traditionally problematic binding site barrier was used to induce potent apoptosis within the tumor nest with only a single conventional gene therapy agent, (2) the fibroblasts *in situ* were not only engineered to secrete a cytotoxic protein but also mechanistically reprogrammed to be tumor suppressive in a feedback fashion and (3) lastly, reprogramming of fibroblasts paved the way for coupling signal-dependent stromal reprogramming with tumor-directed cytotoxic NPs and perhaps immunologic drugs, offering a new paradigm in the treatment of desmoplastic tumors. Furthermore, fibroblasts could be engineered to produce various cytokines, orchestrating the suppressive microenvironment to achieve a more sustained antitumor response. In the real clinical cases, the ECM content may vary among different individuals, as well as the ratio of stroma cells/tumor cells. All these factors would affect the potency of NPs delivery to fibroblasts and the efficacy of protein production in fibroblasts. Therefore, with regard to future clinical application, the combination of our conceptual strategy with individualized therapy would be more promising.

Supplementary Material

Refer to Web version on PubMed Central for supplementary material.

Acknowledgments

The work was supported by NIH grants CA149363, CA151652, and CA149387, and by the North Carolina Biotech Center Institutional Support Grant 2005-IDG-1016.

We thank Dr. Shawn Hingtgen (UNC) for providing the sTRAIL plasmid. We acknowledge UNC Animal Histopathology Core and UNC Translational Pathology Laboratory for tissue embedding, IF and IHC staining. We thank UNC-CH Genome Core for gene sequencing of sTRAIL and TRAIL. We also appreciate the help of UNC Flow Cytometry Core, the ICP-MS Core and UNC CHANL for cell sorting, platinum quantification, and TEM imaging. We appreciate Dr. Yi Zhao (UNC) and Dr. Sai An (UNC)’s help with the manuscript revision.

References

1. Ernsting MJ, Hoang B, Lohse I, Undzys E, Cao P, Do T, et al. Targeting of metastasis-promoting tumor-associated fibroblasts and modulation of pancreatic tumor-associated stroma with a carboxymethylcellulose-docetaxel nanoparticle. Journal of controlled release : official journal of the Controlled Release Society. 2015; 206:122–130. [PubMed: 25804872]
2. Miller MA, Zheng YR, Gadde S, Pfirschke C, Zope H, Engblom C, et al. Tumour-associated macrophages act as a slow-release reservoir of nano-therapeutic Pt(IV) pro-drug. Nature communications. 2015; 6:8692.

3. Miao L, Lin CM, Huang L. Stromal barriers and strategies for the delivery of nanomedicine to desmoplastic tumors. Journal of controlled release : official journal of the Controlled Release Society. 2015; 219:192–204. [PubMed: 26277065]
4. Roode LE, Brighton H, Bo T, Perry JL, Parrott MC, Kersey F, et al. Subtumoral analysis of PRINT nanoparticle distribution reveals targeting variation based on cellular and particle properties. Nanomedicine : nanotechnology, biology, and medicine. 2016
5. Miao L, Wang Y, Lin CM, Xiong Y, Chen N, Zhang L, et al. Nanoparticle modulation of the tumor microenvironment enhances therapeutic efficacy of cisplatin. Journal of controlled release : official journal of the Controlled Release Society. 2015; 217:27–41. [PubMed: 26285063]
6. Smith NR, Baker D, Farren M, Pommier A, Swann R, Wang X, et al. Tumor Stromal Architecture Can Define the Intrinsic Tumor Response to VEGF-Targeted Therapy. Clinical Cancer Research. 2013; 19(24):6943–6956. [PubMed: 24030704]
7. LeBeau AM, Brennen WN, Aggarwal S, Denmeade SR. Targeting the cancer stroma with a fibroblast activation protein-activated promelittin protoxin. Mol Cancer Ther. 2009; 8(5):1378–1386. [PubMed: 19417147]
8. Murakami M, Ernsting MJ, Undzys E, Holwell N, Foltz WD, Li SD. Docetaxel Conjugate Nanoparticles That Target alpha-Smooth Muscle Actin-Expressing Stromal Cells Suppress Breast Cancer Metastasis. Cancer research. 2013; 73(15):4862–4871. [PubMed: 23907638]
9. Sherman MH, Yu RT, Engle DD, Ding N, Atkins AR, Tiriac H, et al. Vitamin D receptor-mediated stromal reprogramming suppresses pancreatitis and enhances pancreatic cancer therapy. Cell. 2014; 159(1):80–93. [PubMed: 25259922]
10. Moffitt RA, Marayati R, Flate EL, Volmar KE, Loeza SG, Hoadley KA, et al. Virtual microdissection identifies distinct tumor- and stroma-specific subtypes of pancreatic ductal adenocarcinoma. Nature genetics. 2015; 47(10):1168–1178. [PubMed: 26343385]
11. De Palma M, Lewis CE. Macrophage regulation of tumor responses to anticancer therapies. Cancer cell. 2013; 23(3):277–286. [PubMed: 23518347]
12. Yoo J, Choi S, Hwang KS, Cho WK, Jung CR, Kwon ST, et al. Adeno-associated virus-mediated gene transfer of a secreted form of TRAIL inhibits tumor growth and occurrence in an experimental tumor model. The journal of gene medicine. 2006; 8(2):163–174. [PubMed: 16144019]
13. Zhang X, Edwards JP, Mosser DM. The expression of exogenous genes in macrophages: obstacles and opportunities. Methods in molecular biology. 2009; 531:123–143. [PubMed: 19347315]
14. Voortman J, Resende TP, Abou El Hassan MA, Giaccone G, Kruyt FA. TRAIL therapy in non-small cell lung cancer cells: sensitization to death receptor-mediated apoptosis by proteasome inhibitor bortezomib. Molecular cancer therapeutics. 2007; 6(7):2103–2112. [PubMed: 17620439]
15. O'Leary L, van der Sloot AM, Reis CR, Deegan S, Ryan AE, Dhami SP, et al. Decoy receptors block TRAIL sensitivity at a supracellular level: the role of stromal cells in controlling tumour TRAIL sensitivity. Oncogene. 2015
16. Shah K, Tung CH, Yang K, Weissleder R, Breakefield XO. Inducible release of TRAIL fusion proteins from a proapoptotic form for tumor therapy. Cancer research. 2004; 64(9):3236–3242. [PubMed: 15126365]
17. Wang Y, Xu Z, Guo S, Zhang L, Sharma A, Robertson GP, et al. Intravenous delivery of siRNA targeting CD47 effectively inhibits melanoma tumor growth and lung metastasis. Molecular therapy : the journal of the American Society of Gene Therapy. 2013; 21(10):1919–1929. [PubMed: 23774794]
18. Miao L, Guo S, Zhang J, Kim WY, Huang L. Nanoparticles with Precise Ratiometric Co-Loading and Co-Delivery of Gemcitabine Monophosphate and Cisplatin for Treatment of Bladder Cancer. Advanced functional materials. 2014; 24(42):6601–6611. [PubMed: 25395922]
19. Zhang J, Miao L, Guo S, Zhang Y, Zhang L, Satterlee A, et al. Synergistic anti-tumor effects of combined gemcitabine and cisplatin nanoparticles in a stroma-rich bladder carcinoma model. Journal of controlled release : official journal of the Controlled Release Society. 2014; 182:90–96. [PubMed: 24637468]
20. Fatin-Rouge NSK, Buffle J. Size Effects on Diffusion Processes within Agarose Gels. Biophys J. 2004; 86(5):10. [PubMed: 14695245]

21. Dasargyri A, Hervella P, Christiansen A, Proulx ST, Detmar M, Leroux JC. Findings questioning the involvement of Sigma-1 receptor in the uptake of anisamide-decorated particles. Journal of controlled release : official journal of the Controlled Release Society. 2016; 224:229–238. [PubMed: 26774218]
22. Hingtgen S, Ren XH, Terwilliger E, Masson M, Weissleder R, Shah K. Targeting multiple pathways in gliomas with stem cell and viral delivered S-TRAIL and Temozolomide. Molecular cancer therapeutics. 2008; 7(11):3575–3585. [PubMed: 19001440]
23. Shah K, Tung CH, Yang K, Weissleder R, Breakefield XO. Inducible release of TRAIL fusion proteins from a proapoptotic form for tumor therapy. Cancer research. 2004; 64(9):3236–3242. doi. [PubMed: 15126365]
24. Chono S, Li SD, Conwell CC, Huang L. An efficient and low immunostimulatory nanoparticle formulation for systemic siRNA delivery to the tumor. Journal of controlled release : official journal of the Controlled Release Society. 2008; 131(1):64–69. [PubMed: 18674578]
25. Lu P, Weaver VM, Werb Z. The extracellular matrix: a dynamic niche in cancer progression. J Cell Biol. 2012; 196(4):395–406. [PubMed: 22351925]
26. Straussman R, Morikawa T, Shee K, Barzily-Rokni M, Qian ZR, Du J, et al. Tumour micro-environment elicits innate resistance to RAF inhibitors through HGF secretion. Nature. 2012; 487(7408):7500–7504.
27. Incio J, Suboj P, Chin SM, Vardam-Kaur T, Liu H, Hato T, et al. Metformin Reduces Desmoplasia in Pancreatic Cancer by Reprogramming Stellate Cells and Tumor-Associated Macrophages. PloS one. 2015; 10(12):e0141392. [PubMed: 26641266]
28. Ungefroren H, Kruse ML, Trauzold A, Roeschmann S, Roeder C, Arlt A, et al. FAP-1 in pancreatic cancer cells: functional and mechanistic studies on its inhibitory role in CD95-mediated apoptosis. Journal of cell science. 2001; 114(Pt 15):2735–2746. [PubMed: 11683408]
29. Novak M, Leonard MK, Yang XH, Kowluru A, Belkin AM, Kaetzel DM. Metastasis suppressor NME1 regulates melanoma cell morphology, self-adhesion and motility via induction of fibronectin expression. Experimental dermatology. 2015; 24(6):455–461. [PubMed: 25808322]
30. Hawinkels LJ, Paauwe M, Verspaget HW, Wiercinska E, van der Zon JM, van der Ploeg K, et al. Interaction with colon cancer cells hyperactivates TGF-beta signaling in cancer-associated fibroblasts. Oncogene. 2014; 33(1):97–107. [PubMed: 23208491]
31. Zhu Y, Yin WL, Ba YF, Tian L, Gu ZQ, Zhang MS, et al. Transforming growth factor-1 promotes the transcriptional activation of plasminogen activator inhibitor type 1 in carcinoma-associated fibroblasts. Molecular medicine reports. 2012; 6(5):1001–1005. [PubMed: 22895748]
32. Cantarella G, Risuglia N, Dell'eva R, Lempereur L, Albini A, Pennisi G, et al. TRAIL inhibits angiogenesis stimulated by VEGF expression in human glioblastoma cells. British journal of cancer. 2006; 94(10):1428–1435. [PubMed: 16622457]
33. Griffon-Etienne G, Boucher Y, Brekken C, Suit HD, Jain RK. Taxane-induced apoptosis decompresses blood vessels and lowers interstitial fluid pressure in solid tumors: clinical implications. Cancer research. 1999; 59(15):3776–3782. [PubMed: 10446995]
34. Jain RK. Normalization of tumor vasculature: an emerging concept in antiangiogenic therapy. Science. 2005; 307(5706):58–62. [PubMed: 15637262]
35. Carmeliet P, Jain RK. Principles and mechanisms of vessel normalization for cancer and other angiogenic diseases. Nature reviews Drug discovery. 2011; 10(6):417–427. [PubMed: 21629292]
36. Meijer TW, Kaanders JH, Span PN, Bussink J. Targeting hypoxia, HIF-1, and tumor glucose metabolism to improve radiotherapy efficacy. Clinical cancer research : an official journal of the American Association for Cancer Research. 2012; 18(20):5585–5594. [PubMed: 23071360]
37. Zhang X, Dong Y, Zeng X, Liang X, Li X, Tao W, et al. The effect of autophagy inhibitors on drug delivery using biodegradable polymer nanoparticles in cancer treatment. Biomaterials. 2014; 35(6):1932–1943. [PubMed: 24315578]
38. Chauhan VP, Stylianopoulos T, Martin JD, Popovic Z, Chen O, Kamoun WS, et al. Normalization of tumour blood vessels improves the delivery of nanomedicines in a size-dependent manner. Nat Nanotechnol. 2012; 7(6):383–388. [PubMed: 22484912]

39. Guo S, Wang Y, Miao L, Xu Z, Lin CM, Zhang Y, et al. Lipid-coated Cisplatin nanoparticles induce neighboring effect and exhibit enhanced anticancer efficacy. ACS nano. 2013; 7(11):9896–9904. [PubMed: 24083505]
40. Cabral H, Matsumoto Y, Mizuno K, Chen Q, Murakami M, Kimura M, et al. Accumulation of sub-100 nm polymeric micelles in poorly permeable tumours depends on size. Nat Nanotechnol. 2011; 6(12):815–823. [PubMed: 22020122]
41. Kano MR, Bae Y, Iwata C, Morishita Y, Yashiro M, Oka M, et al. Improvement of cancer-targeting therapy, using nanocarriers for intractable solid tumors by inhibition of TGF-beta signaling. Proceedings of the National Academy of Sciences of the United States of America. 2007; 104(9): 3460–3465. [PubMed: 17307870]
42. Meng H, Zhao Y, Dong J, Xue M, Lin YS, Ji Z, et al. Two-wave nanotherapy to target the stroma and optimize gemcitabine delivery to a human pancreatic cancer model in mice. ACS nano. 2013; 7(11):10048–10065. [PubMed: 24143858]
43. Matsuzaki H, Schmied BM, Ulrich A, Standop J, Schneider MB, Batra SK, et al. Combination of tumor necrosis factor-related apoptosis-inducing ligand (TRAIL) and actinomycin D induces apoptosis even in TRAIL-resistant human pancreatic cancer cells. Clinical cancer research : an official journal of the American Association for Cancer Research. 2001; 7(2):407–414. [PubMed: 11234897]
44. Kimura J, Ono HA, Kosaka T, Nagashima Y, Hirai S, Ohno S, et al. Conditionally replicative adenoviral vectors for imaging the effect of chemotherapy on pancreatic cancer cells. Cancer science. 2013; 104(8):1083–1090. [PubMed: 23679574]
45. Kircheis R, Schuller S, Brunner S, Ogris M, Heider KH, Zauner W, et al. Polycation-based DNA complexes for tumor-targeted gene delivery in vivo. The journal of gene medicine. 1999; 1(2): 111–120. [PubMed: 10738575]
46. De Vlieghere E, Verset L, Demetter P, Bracke M, De Wever O. Cancer-associated fibroblasts as target and tool in cancer therapeutics and diagnostics. Virchows Archiv : an international journal of pathology. 2015; 467(4):367–382. [PubMed: 26259962]
47. Cirri P, Chiarugi P. Cancer-associated-fibroblasts and tumour cells: a diabolic liaison driving cancer progression. Cancer metastasis reviews. 2012; 31(1–2):195–208. [PubMed: 22101652]
48. Kim SM, Lim JY, Park SI, Jeong CH, Oh JH, Jeong M, et al. Gene Therapy Using TRAIL-Secreting Human Umbilical Cord Blood-Derived Mesenchymal Stem Cells against Intracranial Glioma. Cancer research. 2008; 68(23):9614–9623. [PubMed: 19047138]
49. Islam SS, Mokhtari RB, El Hout Y, Azadi MA, Alauddin M, Yeger H, et al. TGF-beta1 induces EMT reprogramming of porcine bladder urothelial cells into collagen producing fibroblasts-like cells in a Smad2/Smad3-dependent manner. Journal of cell communication and signaling. 2014; 8(1):39–58. [PubMed: 24338442]
50. Bissell MJ, Hines WC. Why don't we get more cancer? A proposed role of the microenvironment in restraining cancer progression. Nat Med. 2011; 17(3):320–329. [PubMed: 21383745]

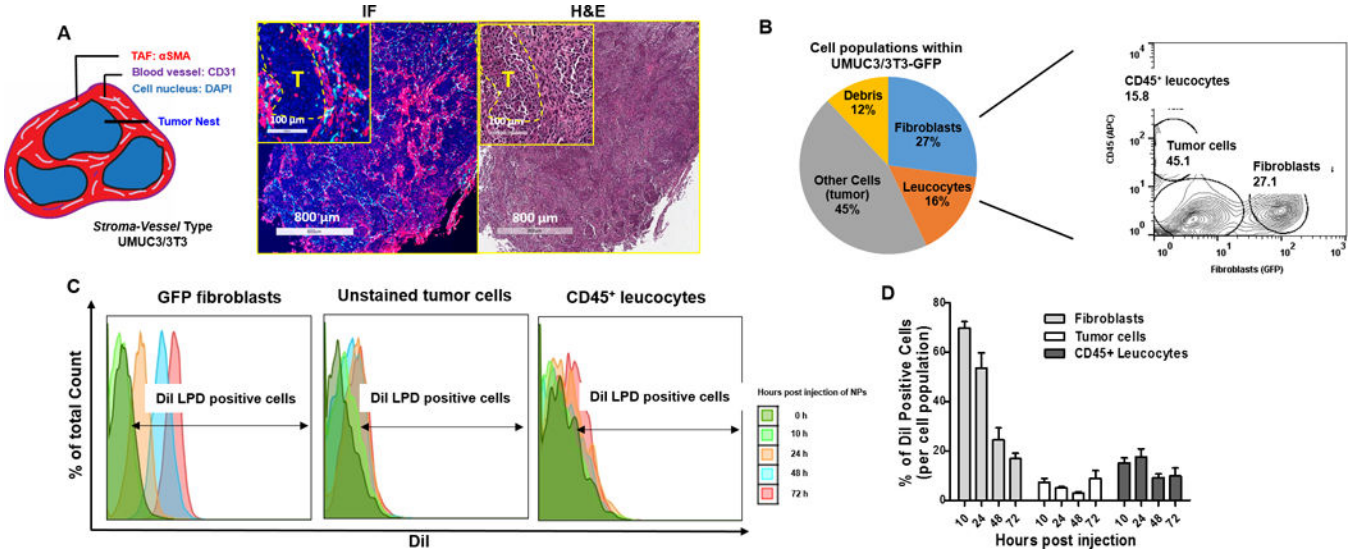

Figure 1. Cell populations that take up LPD in the *stroma-vessel* type desmoplastic tumors

A. The schematic architecture of *stroma-vessel* tumors. Immunofluorescence (IF) and H&E (adjacent section of IF) images (on the right) show the histology of a *stroma-vessel* tumor model: UMUC3/3T3. Examination revealed nests of tumor cells (yellow dotted circles in the inserted magnified images, labeled as T), surrounded by fibrotic components (filled by αSMA positive myofibroblasts, shown in red) between them. CD31 positive blood vessels (shown in cyan) were embedded in the interstitium near myofibroblasts, almost no vessels were observed inside the nests of tumor cells. B. Flow cytometry gating of the cell populations in the UMUC3/3T3-GFP tumors. C. Flow cytometry histograms of the percentage of cells that took up DiI-labeled LPD in each cell population at determined time points. D. Quantitation of the percentage of DiI positive cells in each population (based on the flow data), n = 4.

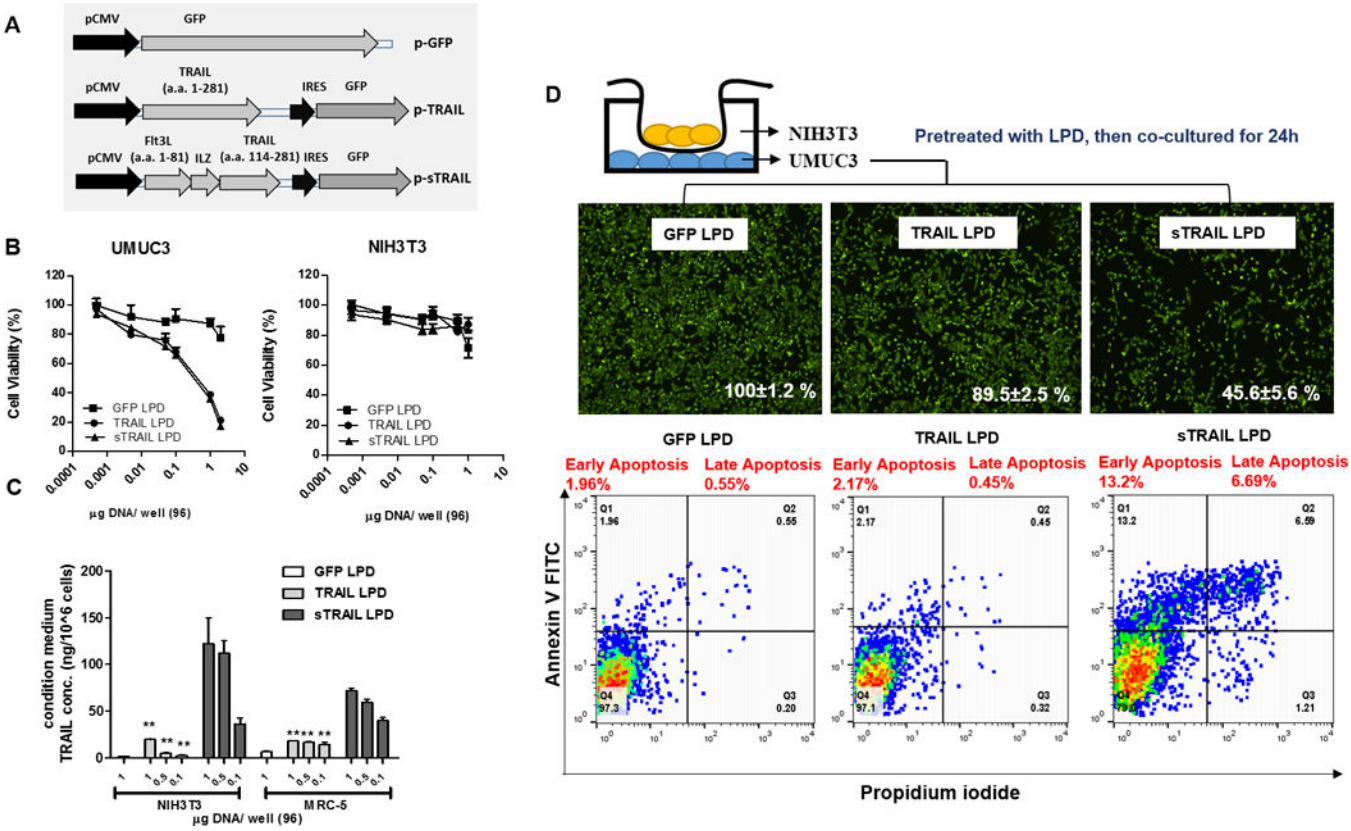

Figure 2. Secretable TRAIL produced by fibroblasts induces apoptosis of neighboring UMUC3 tumor cells

A. Schematic representation of plasmid encoding green fluorescence protein (GFP) fused with sTRAIL or TRAIL (as a less secretable control). B. Cell proliferation of cancer cells, UMUC3 and fibroblasts, NIH3T3 transfected with TRAIL, sTRAIL, GFP at different concentrations (MTT assay, n = 4). UMUC3 cells are sensitive to both TRAIL and sTRAIL, while NIH3T3 are resistant. C. The releasing of sTRAIL protein into the supernatant was determined using ELISA (against TRAIL). Both NIH3T3 and MRC-5 (lung fibroblasts) transfected with sTRAIL secreted TRAIL protein. However, minimal soluble TRAIL was detected in both cell line when transfecting with TRAIL (n = 3, ** $P < 0.01$, compared to sTRAIL LPD treatment). D. The neighboring effect of the sTRAIL protein was determined by a non-contact co-culture study. After co-cultured for 24 h, the UMUC3 cells in the bottom were counted. Cells were visualized by Calcein AM staining (shown in green). Numbers in white calculated the % of total cells in each treatment compared to the total tumor cells in the GFP LPD group. Apoptosis of bottom UMUC3 cells were assessed using annexin V/PI staining and flow cytometry (n = 3).

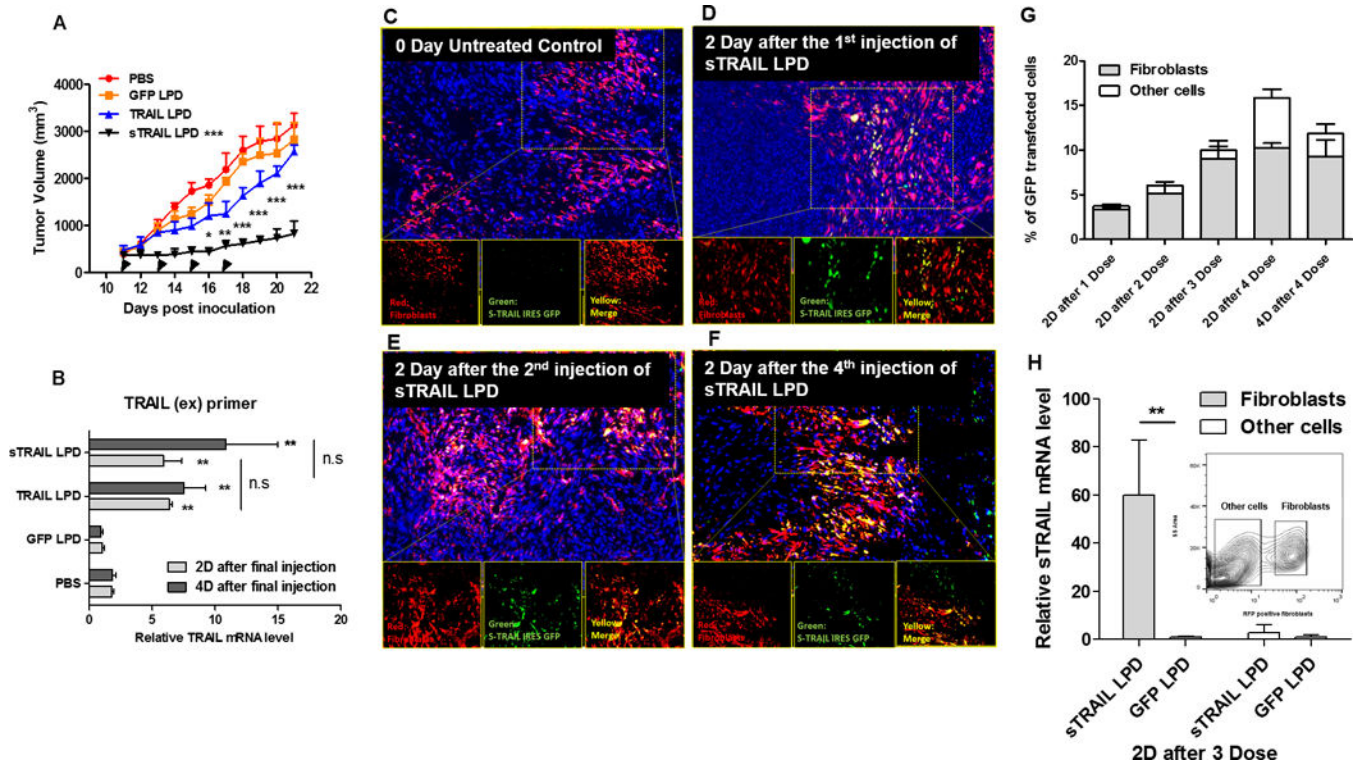

Figure 3. Intravenous injection of sTRAIL LPD leads to the expression of sTRAIL in fibroblasts *in situ*, inhibiting *stroma-vessel* UMUC3/3T3 tumor growth

A, Tumor inhibition curve of mice bearing desmoplastic UMUC/3T3 tumors. Mice were treated with PBS, GFP LPD, TRAIL LPD or sTRAIL LPD (50 μg plasmid/mice), for 4 times (n = 6~8, * $P < 0.05$, ** $P < 0.01$, *** $P < 0.001$, in the legend, compared to PBS group; in the data, compared to each time point of the TRAIL LPD group). B. qPCR quantitation of relative mRNA levels of TRAIL or sTRAIL in the treated tumors. The primers simultaneously for the extracellular domain of TRAIL and sTRAIL were used for the detection (n = 6, ** $P < 0.01$, n.s, no significant difference, compared to PBS group). C-F, IF staining of GFP (shown green), RFP-fibroblasts (shown red) and cell nuclei (DAPI, shown blue) at indicated time points after treatments on cryo-tumor (UMUC3/3T3-RFP) tissues collected. Results showed that the majority of expression of GFP fusion protein co-localized with the RFP-labeled fibroblasts. G. Flow cytometry analysis of GFP's association with RFP-fibroblasts at indicated time points in the dissociated cells from the collected tumor tissues (n = 4). The association of GFP in fibroblasts increased dose-dependently. H. One day after 3 doses of sTRAIL LPD, the RFP-labeled fibroblasts were sorted by flow cytometry. sTRAIL mRNA level in the RFP-labeled fibroblasts and other unlabeled cells were analyzed and compared with the GFP LPD treated group (n = 4, ** $P < 0.01$). The inserted chart indicates gating of the RFP fibroblasts

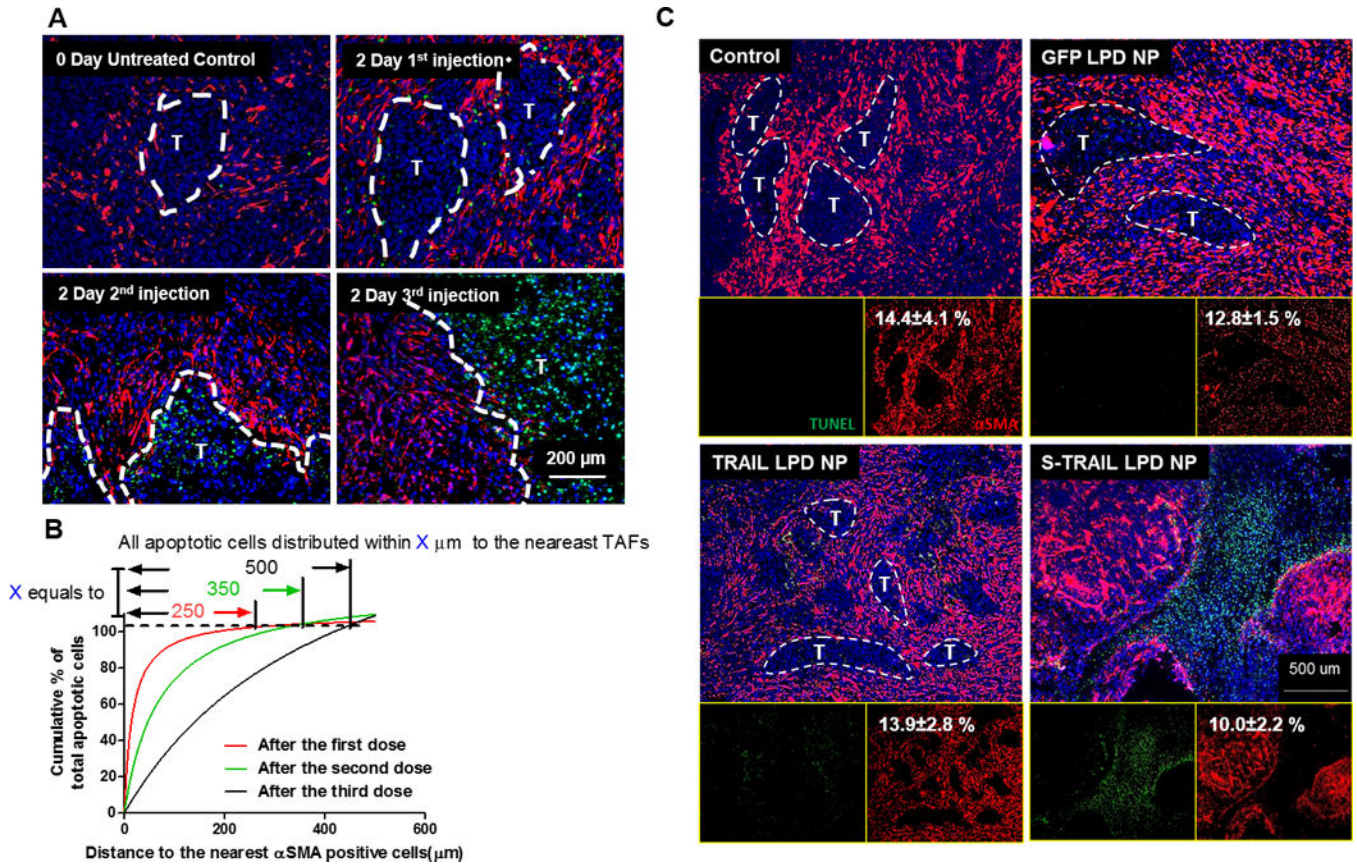

Figure 4. Fibroblasts (*in situ*) that secreted TRAIL induced the apoptosis of neighboring tumor cells

A. IF staining of αSMA and TUNEL from tumor tissues (paraffin-embedded sections) after dose escalation of sTRAIL LPD NPs. Dashed lines indicate edge of the tumor nests. B. Quantification of relative apoptotic cells' distance from the nearest αSMA positive fibroblasts after different doses of sTRAIL LPD NPs. Numbers on top indicate the furthest distance of apoptotic cells to αSMA after different treatments. C. Paraffin-embedded tissues sections from UMUC3/3T3 tumors 2 days after final treatments were stained for αSMA (red, TAFs) and TUNEL (green, apoptosis). The % of αSMA coverage was quantified using Image J and presented as numbers in white on the left corner of each panel. Well-structured tumor nests are highlighted in the images. sTRAIL LPD NPs lead to the disruption of tumor nests and remodeling of the tumor microenvironment.

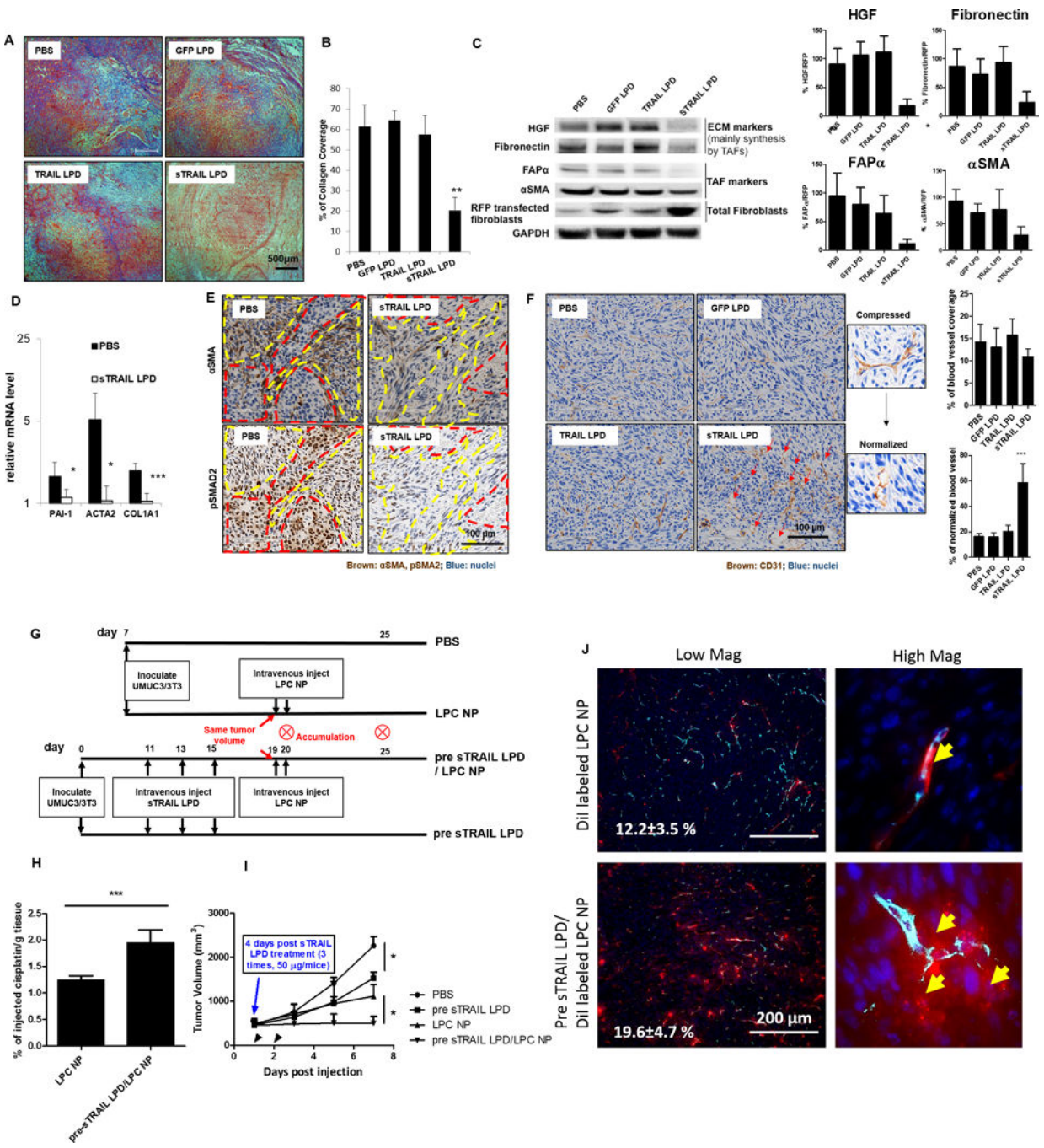

Figure 5. sTRAIL LPD induces the reprogramming of residual fibroblasts and remodeling of TME, facilitating the delivery and antitumor effect of a second-wave nanoformulated cisplatin

A. Masson's trichrome staining of the collagen after endpoint treatments. B. Quantification of the trichrome staining (n = 5, ** $P < 0.01$, compared to PBS group). C. Western blot analysis of the TME markers mainly secreted by TAFs and TAF markers. Intensities of each ECM protein were calculated by comparing to the RFP-transfected fibroblasts and shown on right. Protein/RFP ratios in the PBS group were set as 1 (n = 3, * $P < 0.05$, ** $P < 0.01$, compared to the PBS group). D. mRNA levels of TAF markers in the sorted RFP-fibroblasts after sTRAIL treatment (n = 5, * $P < 0.05$, *** $P < 0.01$, compared to the PBS group). E.

Immunohistochemistry (IHC) staining of αSMA and pSMAD2 in the adjacent sections of PBS and sTRAIL LPD groups. Red dotted circles indicate tumor nests; yellow dotted circles indicate fibroblasts. F. IHC staining of blood vessel (CD31, shown as brown) after different treatments. sTRAIL LPD induces decompression of blood vessels. Red arrows indicate the decompressed vessels. % of blood vessel coverage and % of normalized blood vessels were quantified using image J and showed on right (n = 4, *** $P < 0.001$) (G). Dosing schedule of the second-wave chemotherapy. (H) ICP-MS analysis of cisplatin accumulation after a single dose of cisplatin NP (LPC NP) in mice pre-treated with sTRAIL LPD or without pre-treatment (n = 5, *** $P < 0.001$). (I) Tumor inhibition curve of LPC NP (cisplatin, 1.9 mg/kg) after treating the tumors with sTRAIL LPD (n = 5, * $P < 0.05$). (J) Fluorescence images of the intratumoral distribution of DiI-labeled LPC NP after pretreating tumors with sTRAIL LPD. Blood vessels were stained with CD31 (Cyan). Numbers in white indicate the average % of DiI positive cells in the selected views. Yellow arrows in magnified images demonstrate the extravasation of DiI-NP from the blood vessels.

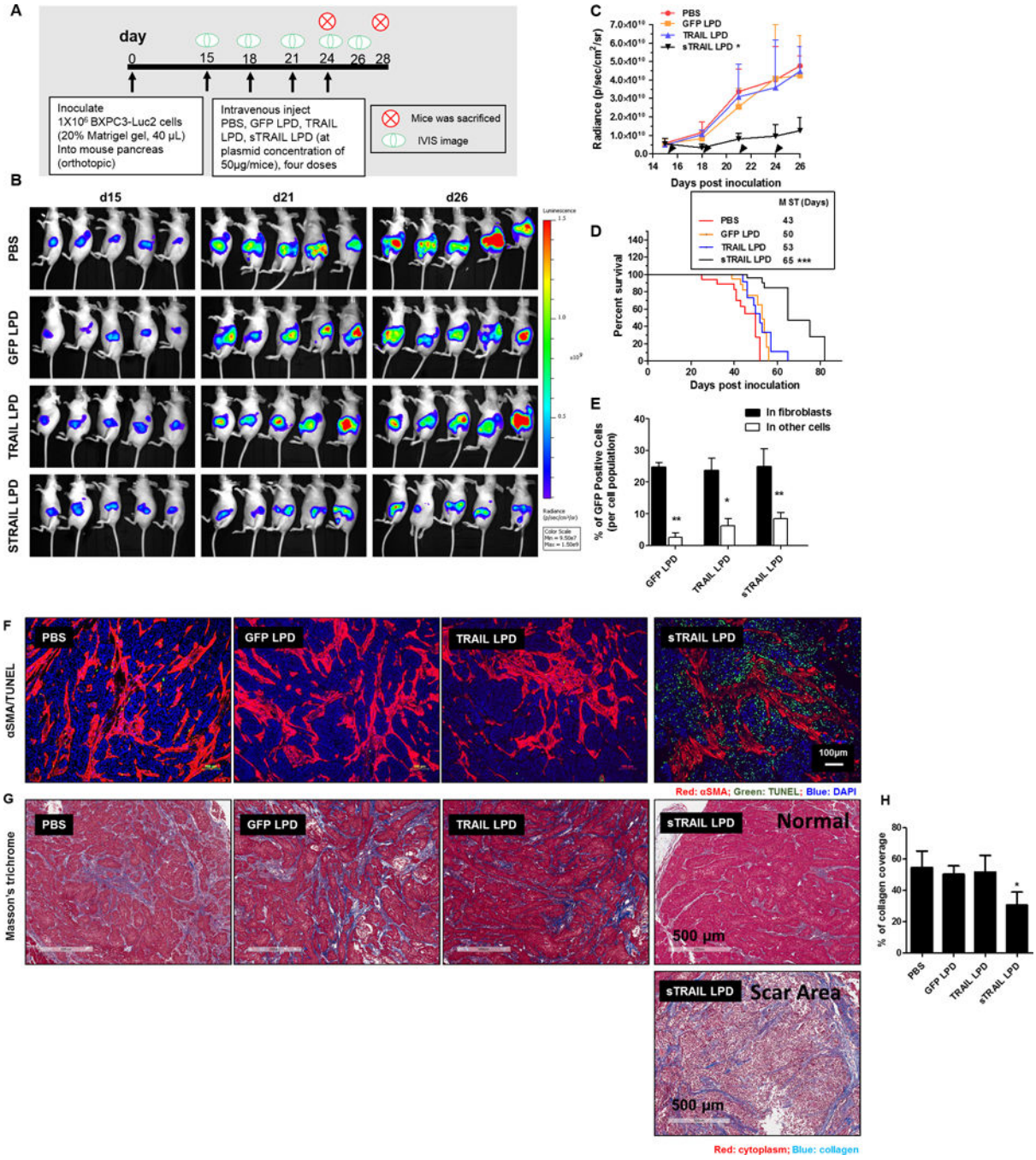

Figure 6. Intravenous administration of sTRAIL LPD inhibited the orthotopic desmoplastic BXPC3 tumor growth and remodeled the tumor microenvironments

A. Dosing schedule of sTRAIL treatment on BXPC3-Luc2. B. IVIS images of BXPC3-Luc2 tumor after different treatments (n = 5). C. Tumor inhibition curve of BXPC3 (n = 6–10, *P < 0.05 compared to PBS group). (D) The survival proportions of the treated groups. Median survival time (MST) are presented in the inserted form (Data shown as mean ± SD, n= 6–8. ***, P < 0.001). E. Flow cytometry analysis of GFP's association with αSMA positive fibroblasts 2 days after the third injection of the LPD (n = 4, * P < 0.05, ** P < 0.01). F. IF staining of αSMA and TUNEL assay from BXPC3-Luc2 tumor tissues after different

treatments. G. Masson's trichrome staining for collagen from the BXPC3-Luc2 tumors after different treatments. Heterogeneities are observed in the sTRAIL LPD groups. Scar tissue (with few cell structures) is observed. H. The quantification of collagen levels based on non-scar area (n = 4~5, * $P < 0.05$).

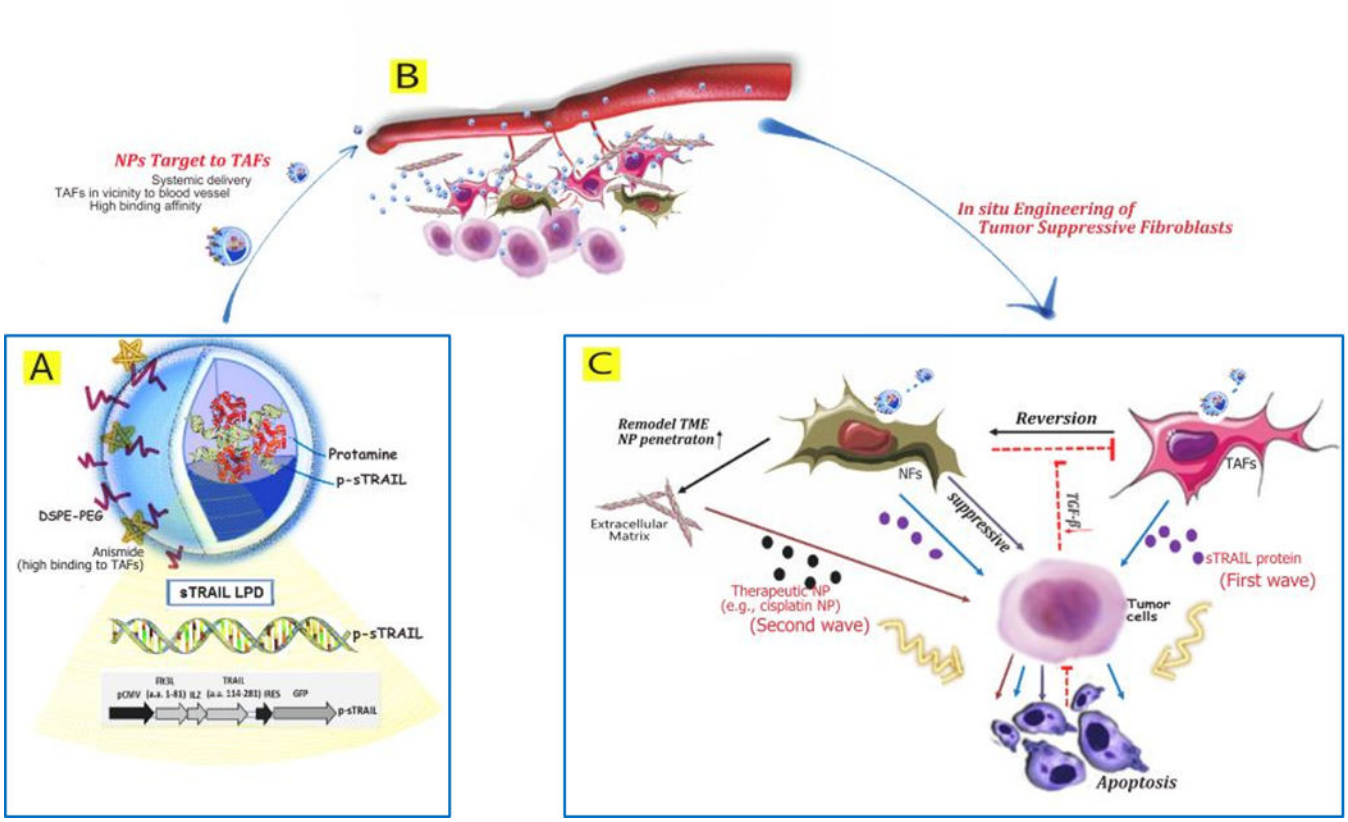

Figure 7. Proposed mechanism of targeting TAFs for *in situ* engineering

A. Plasmid encoding secretable TRAIL protein is condensed with protamine and further encapsulated into PEGylated liposomes coating with anisamide targeting motif (LPD). Diagram of the p-sTRAIL LPD is shown. B. LPD is systemically delivered to tumor region, and then extravasated from blood vessel due to the EPR effect. In most desmoplastic tumors, a thick layer of fibroblasts wraps around the blood vessel. Tumor-associated fibroblasts (TAFs) are the major cells taken up the targeted LPD. C. sTRAIL protein is synthesized by TAFs and diffuses to the neighboring tumor cells. Apoptotic tumor cells reciprocally failed to activate local fibroblasts, reverting the TAFs to normal fibroblasts (NFs). NFs can suppress tumor growth on one end, remodel the TME, and increase the penetration of a second wave chemotherapeutic NPs on the other. Collectively, this multi-wave therapy can induce potent growth inhibition of the desmoplastic tumors.